First Year Technical Report

To

The Department of Energy

For The Period

15th Sept. 1996 - 14th Sept. 1997

Project no. DE FG07 96ER45618

"AN ALTERNATIVE HOST MATRIX BASED ON IRON PHOSPHATE GLASSES FOR THE VITRIFICATION OF SPECIALIZED NUCLEAR WASTE FORMS"

Delbert E. Day, Curator's Professor of Ceramic Engineering
Chandra S. Ray, Research Professor of Ceramic Engineering
And
Kanishka Marasinghe, Research Assistant Professor of Physics

23rd Sept. 1997

Department of Ceramic Engineering and
the Graduate Center for Materials Research
University of Missouri-Rolla
Rolla, MO 65409-1170

Ph:573 341 4354
Fx: 573 341 2071

TABLE OF CONTENTS

I. EXECUTIVE SUMMARY

This report briefly summarizes the work undertaken and completed in the first year of a three year (9/15/96 - 9/14/99) DOE project "An Alternative Host Matrix Based on Iron Phosphate Glasses for the Vitrification of Specialized Nuclear Waste Forms", DOE Contract # DOE96ER45617. Objectives of this project are to:

1. investigate the glass composition and processing conditions that yield optimum properties for iron phosphate glasses for vitrifying radioactive waste,
2. determine the atomic structure of iron phosphate glasses and the structure-property relationships,
3. determine how the physical and structural properties of iron phosphate glasses are affected by the addition of simulated high level nuclear waste components, and
4. investigate the process and products of devitrification of iron phosphate waste forms.

The glass forming ability of about 125 iron phosphate melts has been investigated in different oxidizing to reducing atmospheres using various iron oxide raw materials such as Fe_2O_3, FeO, Fe_3O_4, and $FeC_2O_4.2H_2O$. The chemical durability, redox equilibria between Fe(II) and Fe(III), crystallization behavior and structural features for these glasses and their crystalline forms have been investigated using a variety of techniques including Mossbauer spectroscopy, X-ray absorption spectroscopy (XAS), X-ray photoelectron spectroscopy (XPS), Extended x-ray absorption fine structure (EXAFS) and X-ray absorption near edge structure (XANES) analysis, differential thermal and thermogravimetric analysis (DTA/TGA), and X-ray and neutron diffraction.

Iron phosphate glasses containing several common waste components such as Na_2O, Bi_2O_3, Cs_2O, or UO, have been prepared and investigated. The corrosion resistance of several refractory oxides to fluid iron phosphate melts containing significant amounts of simulated high level nuclear waste (HLW) has been investigated as a function of melting temperature and time in order to identify refractory materials best suited for the large scale melting of these glasses.

Mossbauer spectral studies show that irrespective of the fraction of Fe(II) in the starting batch materials, a redox equilibria corresponding to the Fe(II)/[Fe(III)+ Fe(III)] ratio of 0.2 to 0.3 is reached when these batches are melted at 1200°C for up to 2 h in air. Melting in pure oxygen does not significantly change this ratio. However, the Fe(II) content in the glasses increases beyond this

equilibrium value when a reducing gas is introduced and its partial pressure is increased in the melting atmosphere. The glass forming ability of these melts is closely related to the Fe(II) content and is reduced considerably when the Fe(II) content is above about 33%.

The reduced glass forming tendency was also supported by DTA measurements. With increasing Fe(II) content, the DTA crystallization peaks in these glasses become larger and sharper, and move progressively to lower temperatures, which signify a higher rate of crystallization. The DTA measurements combined with x-ray diffraction (XRD) analysis show that these glasses generally crystallize to ferrous-ferric pyrophosphate ($Fe_3(P_2O_7)_2$) and ferric pyrophosphate ($Fe_4(P_2O_7)_3$) on heating in an inert atmosphere (nitrogen). The $Fe_3(P_2O_7)_2$ phase oxidizes to ferric orthophosphate, $Fe(PO)_4$, accompanied by a change in color from bluish black to yellowish white when heat treatment is continued in either air or oxygen.

Mossbauer analyses further suggest that the local structure of iron phosphate glasses is close to that of the short range structure of crystalline ($Fe_3(P_2O_7)_2$). All of the Fe(II) ions in the glasses tend to occupy a single type of site whereas the Fe(III) ions appear to occupy two distinctly different sites. The average coordination of the Fe(II) and Fe(III) ions appears to be distorted octahedral. A significant fraction of the -P-O-P- bonds present in conventional phosphate glasses is believed to be replaced by the more hydration resistant -P-O-Fe- bonds in the iron phosphate glasses, thereby, making the iron phosphate glasses more chemically durable. The chemical durability of certain iron phosphate glasses is comparable and, in some instances, even higher than that of borosilicate glasses. Although it is believed that the chemical durability for these glasses deteriorates with increasing Fe(II) content, the limited data to date do not confirm any definite correlation between the chemical durability and the valence state of iron ions.

An iron phosphate glass of approximate batch composition, $40Fe_2O_3$-$60P_2O_5$, mol%, has been shown to accommodate large amounts, up to 40 wt%, of common waste components such as Na_2O, Cs_2O, or UO_2 without much loss in its outstanding chemical durability. The addition of various waste components affects the iron redox equilibria, crystallization, and structure of the iron phosphate glasses in different ways. For example, adding Na_2O tends to reduce the valence state of the iron ions, increases the crystallization tendency (decreases glass formation), drives the coordination of iron ions towards perfect octahedral symmetry, and increases the fraction of bridging

(taking part in -P-O-P- type bonds) oxygens. However, adding UO_2 to the ironphosphate glasses has the opposite effect.

A noteworthy feature of the iron phosphate melts is that they do not chemically attack refractory oxides to the same degree as most fluid phosphate melts. Very little to almost zero corrosion was observed at the melt line when different refractory materials in the form of cylindrical rods were immersed in a melt at 1270°C and rotated at about 10 rpm for 24 hours. While corrosion experiments on various refractory materials in an iron phosphate melt containing varying amounts of high level simulated nuclear waste are still continuing, results obtained to date suggest that iron phosphate glasses can be melted in refractory oxide crucibles, alumina or mullite, without undue corrosion of the refractory. Unlike what is observed for many corrosive phosphate melts, molten iron phosphate glasses do not cause any serious damage to refractory oxides.

Good progress has been made in this research and the results have yielded three publications (Journal of the American Ceramic Society and Journal of Non-Crystalline Solids) and been described in four presentations. Measurements similar to those conducted in the first year for the iron phosphate glasses are planned in the second year for different iron phosphate-based waste forms.

Research collaborations have been established with *Lawrence Berkeley National Laboratory, Argonne National Laboratory,* and the *Naval Research Laboratory* for investigating the structure of the iron phosphate glasses and their waste forms using sophisticated tools such as EXAFS, XANES, Raman, NMR, ESR, Neutron Diffraction and Differential Anomalous Neutron Scattering. The effect of radiation on iron phosphate glasses is being studied in collaboration with *Pacific Northwest nation Laboratory.*

Any questions about the technical contents of this report should be directed to Delbert E. Day, the principal investigator of this project.

II. WORK COMPLETED

1. Sample Preparation

Approximately 125 iron phosphate glasses, as categorized in Table I, have been prepared to date. Compositions and melting conditions of these glasses were selected such that the influence a) the Fe/P ratio, b) valence state of iron ions, c) melting conditions, and d) addition of common waste components on chemical and physical properties and atomic structure of iron phosphate glasses can be studied.

Table I. Categories of iron phosphate glasses melted during year #1 .

Category	Batch Composition (mol%)	Melting Temperature and Atmosphere[a]	# of Compositions
1	$(100\text{-}x)Fe_2O_3\text{-}(x)P_2O_5$ $10 \geq x \geq 50$	1250°C in air	10
2	$40Fe_2O_3\text{-}\ 60P_2O_5$	1250°C in inert atmospheres or under varying redox conditions	25
3	$40Fe_2O_3\text{-}\ 60P_2O_5$	In air @ temperatures ranging from 1100 to 1450°C	5
4	$40[(100\text{-}x)FeO\text{-}(x)Fe_2O_3]$ $60P_2O_5$, $0 \geq x \geq 100$	1250°C in inert atmospheres or under varying redox conditions	30
5	$40Fe_2O_3\text{-}\ 60[(100\text{-}x)P_2O_5\text{-}$ $(x)NH_4H_2PO_4]$, $0 \geq x \geq 100$	As in category 4	10
6	$(100\text{-}x)(40Fe_2O_3\text{-}\ 60P_2O_5)\text{-}$ $(x)MO$ $MO \equiv Na_2O, Cs_2O, Bi_2O_3, UO_2$	In air @ 1250°C	25
7	$(100\text{-}x)(31Fe_3O_4\text{-}\ 69P_2O_5)\text{-}$ $(x)MO$ $MO \equiv Na_2O, UO_2$	As in category 6	10

[a] All batches were melted for approximately 1.5hrs.

2. Chemical Durability Studies

The chemical durability of several binary iron phosphate glasses and those containing selected surrogate waste was investigated by measuring the weight loss of lxlx1 cm samples immersed in distilled water at 90°C for 16 days. Figure 1 compares the weight loss ($g/cm^2/min$) of several iron phosphate glasses with two borosilicate glasses prepared at the Hanford and Savannah River sites. Results to date strongly suggest that iron phosphate glasses can accommodate appreciable quantities (in excess of 35 wt% in certain cases) of a variety of HLW without losing their excellent chemical durability.

3. Structural Studies

3.1. Mössbauer Spectroscopy

A new ASA Mössbauer spectrometer utilizing a 50mC Co-57 source was purchased for this project. Room temperature Mössbauer spectra were measured for all the glass samples and their crystallized counterparts. The spectra obtained for glass samples were fit with the minimum number of broadened paramagnetic doublets necessary, usually eight, to match the absorption envelope with a misfit of less than 0.003. This procedure was used to determine the valence state and approximate coordination of iron ions. More detailed structural information for selected glasses were obtained by fitting their Mössbauer spectra with Voight based arbitrary shape quadrupole splitting distributions (VQSD) [1].

The Mössbauer spectrum obtained at 23°C for a glass of batch composition $4OFe_2O_3$-$6OP_2O_5$ (mol%), see Figure 2, is typical of the spectra obtained for most of the glasses melted in air. Table II gives the valence state of iron ions and Mössbauer hyperfine parameters for several selected samples. Samples A through E, see Table II and Figure 3, show that a redox equilibria corresponding to a Fe(II)/[Fe(II)+Fe(III)] ratio between 0.2 and 0.3 is reached when glasses are melted in air. However, the similarity in the Fe(II)/[Fe(II)+Fe(III)] ratio for glasses A, F, and G, which had the same batch composition but were melted in air, nitrogen, and oxygen, respectively, suggests that the process by which the redox equilibria is reached is independent of the oxygen content in the melting atmosphere.

In contrast, the large fraction of Fe(II) in samples H and J indicates that the Fe(II) content

Table II. Mössbauer hyperfine parameters at 23 °C and the iron valence in glass samples. Iron valence in the starting batch is also given.

Sample	Batch Composition, mol%	Melting Atmosphere	Quenched State	δ (mm/s)		QS (mm/s)		Fe(II) Fraction	
				Fe(II)	Fe(III)	Fe(II)	Fe(III)	Batch	Glass[a]
A	$40Fe_2O_3$-$60P_2O_5$	Air	Glass	1.22	0.38	2.14	0.94	0	0.19
B	$31Fe_3O_4$-$69P_2O_5$	Air	Glass	1.24	0.39	2.11	0.91	0.3	0.24
C	$24FeO$-$24Fe_2O_3$-$52P_2O_5$	Air	Glass	1.24	0.39	2.15	0.95	0.3	0.34
D	$57FeC_2O_4.2H_2O$-$43P_2O_5$	Air	Glass	1.24	0.39	2.14	0.91	1	0.24
E	$31Fe_2O_3$-$23P_2O_5$-$46NH_4H_2PO_4$	Air	Glass	1.24	0.40	2.16	0.90	0	0.35
F	Same as sample A	Nitrogen	Glass	1.20	0.39	2.21	0.87	0	0.22
G	Same as sample A	Oxygen	Glass	1.23	0.41	2.11	0.80	0	0.21
H	Same as sample A	70%FG[b]-30%Air	Glass	1.24	0.40	2.14	0.92	0	0.31
J	Same as sample A	90%FG-10%Air	Glass[c]	1.23	0.40	2.18	0.94	0	0.40
K	Same as sample A	FG	Crystallized[d]					0	1
L	Same as sample E	Flowing Ar	Mixed[e]	1.23	0.39	2.2	0.94	0	0.85
M	Same as sample E	Ar	Crystallized[d]					0	1
N	Same as sample A	Air @ 1100°C	Glass	1.25	0.38	2.06	0.89	0	0.17
O	Same as sample A	Air @ 1450°C	Glass	1.23	0.4	2.15	0.94	0	0.57
P	$26Fe_3O_4$-$59P_2O_5$-$15Na_2O$	Air	Glass	1.23	0.40	2.16	0.88	0.3	0.28
Q	$36Fe_2O_3$-$54P_2O_5$-$10Bi_2O_3$	Air	Glass	1.24	0.40	2.17	0.92	0	0.34
R	$28Fe_2O_3$-$42P_2O_5$-$30Cs_2O$	Air	Glass	1.24	0.39	1.98	0.83	0	0.29
S	$26Fe_3O_4$-$59P_2O_5$-$15UO_2$	Air	Glass	1.19	0.36	2.26	0.92	0.3	0.08

[a] Fe(II)/[Fe(II)+Fe(III)] as obtained from Mössbauer spectra.

[b] Forming gas ($90N_2$-$10H_2$ at%).

[c] A trace amount of crystalline material is evident in the Mössbauer spectrum of this sample.

[d] Sample contains more than one crystalline component so Mössbauer hyperfine parameters are not reported. Mössbauer spectra show no detectable Fe(III).

[e] A thin layer on the top surface and a region at the center of the rectangular sample crystallized. Hyperfine parameters are for the glassy part of the sample.

in the glass can be increased by melting in increasingly reducing atmospheres. Also, the high Fe(II) content (0.34) in sample E shows that the iron valence in the glass is sensitive to the reducing ability of chemicals used in the batch. The batch of glass E contained $NH_4H_2PO_4$ which releases NH, when heated and acts as a reducing agent during melting. In addition, the fraction of Fe(II) in the glass increases with increasing melting temperature, see samples N and O in Table II. Mössbauer spectra of iron phosphate glasses containing simulated waste components indicate that the redox equilibria during melting also depends on the concentration and type of the waste component. For example, Na_2O and Bi_2O_3 appear to reduce the valence of iron ions, whereas, UO_2 and Cs_2O appear to increase the valence of the iron ions, see Table II.

Another important result is the apparent dependence of the glass forming ability of the melt on the valence state of the iron ions in the glass. Surface crystallization appears on air quenched samples containing approximately 40% Fe(II) and the extent of crystallization increases when the Fe(II) fraction is increased further. For example, about 60 vol% of the sample crystallized during quenching when the Fe(II) fraction was 0.85, see samples J, K, and M in Table II.

Controlling the oxidation state of a waste glass melt is important because extreme oxidizing conditions can facilitate the formation of foam on the melt surface which in turn diminishes the heat transfer and lowers the melting rates. On the other hand, extreme reducing conditions can cause the formation of metallic phases which can settle to the melter floor and potentially cause an electric short[2]. During the second year of this project, we will use Mössbauer spectroscopy extensively to further investigate the redox equilibria process in iron phosphate glasses containing selected waste components.

Figure 4(a & b) shows the distribution in the quadrupole splitting obtained by fitting the Mössbauer spectrum of glass B with the Voight based arbitrary shape quadrupole splitting distribution (VQSD) method. The symmetric distribution observed for Fe(II) indicates that Fe(II) ions occupy one type of site. However, the asymmetric distribution for Fe(III), which can be fit with two Gaussians, indicates that there are two types of Fe(III) sites, Fe3S1 and Fe3S2, as shown in Figure 4(a). Quadrupole distributions obtained for glasses containing high Fe(II) fractions suggest that Fe(II) prefers to substitute for the Fe(III) ions occupying the Fe3S1 site as the Fe(II) fraction increases above the equilibrium value of 0.2-0.3, see Figure 4(c). In the coming year we intend to

apply this precise fitting technique (VQSD) to extract information about Fe-O bond distances and coordination symmetry around iron ions and to study how the structural role of the iron ions is influenced by the addition of waste components.

3.2. Extended X-Ray Absorption Fine Structure (EXAFS) and X-Ray Absorption Near Edge Structure (XANES) Measurements.

X-ray absorption spectra (XAS) were collected for several binary iron phosphate glasses, their crystalline counterparts, and several iron phosphate glasses containing simulated waste components on BL 4-1 at the Stanford Synchrotron Radiation Laboratory (SSRL). Fe *K* edge data was collected for all of the samples. U-L edge, Bi-L edge, and Cs-L edge data was collected for glasses containing UO_2, Bi_2O_3, and Cs_2O, respectively. Preliminary analysis of the data for glass B in Table- II (batch composition $31Fe_3O_4$- $69P_2O_5$mol%), it's crystalline counterpart, and several glasses containing Na_2O or UO_2has been carried out using the FEFF6[3] multiple scattering code for all single scattering paths up to Fe-P (-3.4 A).

Figure 5 shows X-ray-absorption near-edge (XANES) data from glass sample B, its crystallized counterpart ($Fe_3(P_2O_7)_2$), and three reference crystalline samples, FeO, Fe_3O_4, and Fe_2O_3. The feature in the pre-edge region near 7114 eV is from a ls-3d transition which is suppressed or minimized if the iron atoms are in perfect octahedral coordination [4]. For instance, this pre-edge feature is very weak for Fe0 which has Fe(II) in undistorted octahedral coordination. In contrast, the pre-edge peak is prominent in the XANES data for Fe_3O_4(Fe(III) ions in perfect octahedral coordination and Fe(II) ion in perfect tetrahedral coordination) and Fe_2O_3(Fe(III) in distorted octahedral sites). As seen in Figure 5, XANES data for the glass sample B and its crystallized counterpart ($Fe_3(P_2O_7)_2$) display the ls-3d pre-edge feature. However, the ls-3d transition is less pronounced in the crystalline sample than in the glass indicating that the octahedral character in the general coordination of iron ions in the glass is less than that in crystalline $Fe_3(P_2O_7)_2$.

Figure 6 shows the Fourier transform (FT) of $k^3\chi(k)$, where $\chi(k)=(\mu(k)-\mu_0(k))/\mu_0(k)$ and k is the photoelectron wave vector given by $E-E_0=\hbar^2k^2/2m_e$, and μ is the absorption, obtained from extended x-ray-absorption fine-structure (EXAFS) data for glass sample B and its crystallized counterpart. The fit to the Fourier transform of the data for the crystallized sample is consistent with

the crystal structure of $Fe_3(P_2O_7)_2$. The same crystal structure was used as a starting guide in fitting the Fourier transform of the data for the glass sample. Fit parameters given in Table III indicate that the near-neighbor environment ($r \lesssim 2.4$Å) around iron ions in the glass and crystalline $Fe_3P_2O_7)_2$ are not very different. Especially, the parameters in Table 5 support a structural model in which a majority of the oxygen atoms in the glass take part in -Fe-O-P- type bonds as is the case in crystalline $Fe_3(P_2O_7)_2$.

Fe *K* near edge absorption data for sample B and for samples containing Na_2O and UO_2 is shown in Figure 7. The ls-3d transition in the glasses shows that as UO_2 is added to the base glass, the oxygen coordination around iron becomes more distorted as compared to a perfect octahedron, yet as Na_2O is added, the iron coordination becomes more like a regular octahedron. The glass sample with 15wt% Na_2O has a transition that is nearly as small as the transition previously measured[5] in crystalline $Fe_3(P_2O_7)_2$.

Table III. Parameters obtained by fitting the Fourier transforms of EXAFS data for glass sample B and its crystallized counterpart.<*N*> is the number of neighbor atoms in each shell. σ is the Debye-Wailer parameter and measurements of dV> assume an $S_0^2=0.75$, estimated from the reference compounds. Numbers in parenthesis are the errors in the last specified digit.

Shell	Crystallized Sample			Glass Sample		
	<*N*>	*R*(Å)	σ(Å)	<*N*>	*R*(Å)	σ(Å)
Fe-O	3.0(3)	1.91(1)	0.073(5)	3.4(4)	1.9(1)	0.070(5)
Fe-O	2.0(6)	2.12(3)	0.07(1)	0.8(2)	2.11(3)	0.08(2)
Fe-O	0.8(3)	2.41(3)	0.07(1)	0.6(2)	2.35(5)	0.07(2)
Fe-Fe	1.0(3)	2.97(5)	0.09(2)	0.2(1)	3.2(1)	0.07(3)
Fe-P	6(2)	3.43(5)	0.09(3)	3.1(7)	3.18(4)	0.09(2)
Fe-P				3.1(7)	3.41(4)	0.09(2)

X-ray absorption spectroscopy is a powerful technique for probing the local structure of a glass. This technique can be used to investigate how the waste atoms are situated within the glass matrix. During the next phase of this project, we intend to complete the analysis of the excellent data we have already obtained. We will also collect XAS data for glasses containing a wide spectrum of waste components.

3.3. X-Ray Photoelectron Spectroscopy

XPS data was collected on a Physical Electronics model 548 spectrometer at a pass energy of 50eV using Mg Kα (hν= 1254.6 eV) radiation . In order to minimize contamination, samples were fractured in-situ under high vacuum (~ 1 0^{-8} torr) just before analysis. The O1s spectrum of glasss A shown in Figure 8 can be fit using two Gaussians, one assigned to the bridging oxygens involved in -P-O-P- bonds and the other assigned [6] to the remaining of the oxygens, with relative areas of approximately 15% and 85%, respectively. This is consistent with a glass structure which has only a small fraction of bridging (-P-O-P-) oxygens as is the case in crystalline compound $Fe_3(P_2O_7)_2$.

Table IV. O1s XPS parameters for three iron phosphate glasses.

Batch Composition (mol%)	% Area of Voight Peak	
	Bridging Oxygens	Other Oxygens
$28Fe_3O_4$-$62P_2O_5$-$10Na_2O$	30	70
$31Fe_3O_4$-$69P_2O_5$	15	85
$26Fe_3O_4$-$59P_2O_5$-$15UO_2$	12	88

XPS fit parameters for iron phosphate glasses containing Na_2O or UO_2, see Table IV, suggest that adding Na_2O or UO_2 to iron phosphate glasses affects the glass structure in opposite ways. Addition of UO_2 appears to decrease the number of bridging oxygens (-P-O-P-), whereas, adding Na_2O appears to increase it. The latter result, where the fraction of bridging oxygens (-P-O-P-) appears to increase with increasing Na_2O content , is unusual and must be further investigated. Because non-bridging oxygens (-Fe-O-P-) are more hydration resistant than bridging oxygens, the

bridging to non-bridging oxygen ratio in iron phosphate glasses is expected to play a major role in their chemical durability. We will continue to use XPS techniques to investigate how the structural role of oxygen is affected by the addition of various waste components.

3.4. Neutron Diffractions Studies.

Low-Q neutron diffraction data was collected for glass B, see Table II, and several iron phosphate glasses containing UO_2 at the Intense Pulsed Neutron Source, Argonne National Laboratory. This data will be analyzed during the second year of this project. In addition, neutron diffraction and differential anomalous scattering data will be collected for iron phosphate glasses containing surrogate high level waste components.

3.5. Differential Thermal Analysis (DTA) and Thermogravimetric Analysis (TGA).

3.51. Binary Iron-Phosphate Masses:

The crystallization behavior of these glasses was investigated using a Perkin Elmer DTA-7 instrument at a heating rate of **10° C/min** in an atmosphere of flowing (30 cm^3/min) nitrogen gas. A typical sample weight of about 40 mg of 200 mesh particles, as was used for Mossbauer measurements, was used for the DTA measurements. The DTA thermograms for all the binary iron phosphate glasses, generally, look alike, although the temperature, height and width of the glass transition and crystallization peaks change markedly with composition, particularly, with the initial Fe(II) or Fe(III) concentration in the glass.

The DTA pattern shown in Fig. 9 for a $40Fe_2O_3$-$60P_2O_5$, mol%, glass (glass A, Table II), which contains one glass transition and two crystallization peaks is typical of the DTA patterns for the binary iron phosphate glasses investigated to date. Depending upon composition, the glass transition temperature, T,, for these glasses ranged from 490 to 515" C, and the two crystallization temperatures, T_{p1} and T_{p2}, ranged from 575 to 620, and 800 to 830" C, respectively.

As analyzed by XRD, the first or low temperature peak, T_{p1} , corresponds to the crystallization of ferrous-ferric pyrophosphate, $Fe_3(P_2O_7)_4$, and the second or high temperature peak corresponds to the crystallization of ferric pyrophosphate, $Fe_4(P_2O_7)_3$. As expected, therefore, the first peak becomes sharper and larger, and occurs at a lower temperature for compositions containing

higher amounts of Fe(II) (the concentration of Fe(II) in glass A is about 19%). Simultaneously the second peak becomes smaller and shifts to a higher temperature with increasing Fe(II) content.

The ratio of Fe(II)/[Fe(II)+Fe(III)] in $Fe_3(P_2O_7)_2$ is 1:3, which means that a glass containing 33.3% Fe(II) will exhibit only one exothermic peak corresponding to the crystallization of $Fe_3(P_2O_7)_2$. There will be no Fe((III) left for the second crystallization peak (ferric pyrophosphate) to occur. This is clearly demonstrated in Fig. 10 which shows the DTA thermogram for (1) a 31Fe_3O_4-69P_2O_5, mol% (equivalent to 23.7Fe_2O_3-23.7FeO-52.6P_2O_5, mol%, glass B in Table II) and (2) that for the same glass B preheated at 400° C in forming gas for 24 h. The heat treatment in the forming gas reduces some of the Fe(III) ions to Fe(II). The concentration of Fe(II) as measured by Mossbauer spectroscopy was 25% in glass B and was about 34% in the heat-treated glass.

Also, compare the DTA thermograms for the glasses A (Fig. 9) and B (curve (1) in Fig. 10). Since the concentration of Fe(II) in the glass B in Fig. 10 is higher than that of glass A (25% compared 19%) in Fig. 9, the height of the second or high temperature crystallization peak (ferric pyrophosphate) for glass B is smaller than that of glass A.

The color of the iron phosphate glasses is typically black and the color of powdered samples after heating in the DTA experiments in nitrogen is black to bluish black. Careful observation confirmed that the original black color of the glass is retained when only the low temperature $Fe_3(P_2O_7)_2$ phase is crystallized. After crystallization of $Fe_4(P_2O_7)_3$ the color of the sample becomes bluish. However, the samples become white (or yellowish white) when the DTA experiments are performed in flowing air.

XRD analysis of the samples used for DTA measurements in air showed the presence of ferric orthophosphate, $Fe(PO_4)$, in addition to $Fe_4(P_2O_7)_3$ and a small amount of $Fe_3(P_2O_7)_2$. Systematic heat treatment experiments on the powdered glass A at different temperatures in nitrogen and in air for longer periods of time (about 24 h) combined with simultaneous XRD analyses suggest that $Fe_3(P_2O_7)_2$ crystallizes first from this glass at about 580" C in both nitrogen and air and the sample color remains black. At about 800° C in nitrogen, $Fe_4(P_2O_7)_3$ starts crystallizing and the sample color changes to bluish black. In air, a simultaneous crystallization of $Fe_4(P_2O_7)_3$ and a phase transformation from $Fe_3(P_2O_7)_2$ to $Fe(PO_4)$ occur at about 800° C and the sample color changes from predominantly black (or bluish black) to yellowish white. The $Fe(PO_4)$ phase is believed to be

responsible for the yellowish white color of the sample.

The phase transformation from $Fe_3(P_2O_7)_2$ to $FePO_4$ is an oxidation process :

$$Fe_3(P_2O_7)_2 + 1/2O = 3FePO_4 + PO_{2.5}$$

when Fe(II) ions are oxidized to Fe(III) and should be associated with an increase in weight. A thermogravimetric analysis (TGA, Mettler Type-l) conducted in air indeed showed an increase in weight for powders of all the binary iron phosphate glasses. However, no weight increase was observed when the TGA was conducted in nitrogen. As expected, this increase in weight was found to depend on the composition of the glass, more precisely, on the concentration of the Fe(II) ions initially present in the glass. A larger weight increase was observed for a glass containing a higher concentration of Fe(II).

Typical TGA data obtained on heating glass B at 10" C/mm are shown in Fig. 11. The glass starts gaining weight at about 800° C when heated in air, but no measurable weight change is observed when this glass is heated in nitrogen. Mossbauer analysis of this glass crystallized in nitrogen at 800" C (bluish black sample) shows the presence of the same 25% Fe(II) as what was measured in the base glass, but no Fe(II) was detected in the sample crystallized in air at 800° C (yellowish white sample). These Mossbauer results indicate that all the Fe(II) ions present in the glass were oxidized to Fe(III) when the glass was heated in air at 800°C. Calculations show that a complete transformation of $Fe_3(P_2O_7)_2$ to $FePO_4$ in glass B should produce an increase in weight of about 0.88% which is in excellent agreement with the 0.8% weight increase measured by TGA, Fig. 11.

DTA experiments for glass A were also conducted (in nitrogen) at heating rates of 2, 4, 6, 10, and 15" C/min. The data were used to determine the overall activation energy for crystallization, E, using the equation,

$$\ln(T_p^2/\varphi) = E/RT_p + \text{const.},$$

where T_p is the temperature at the maximum of the DTA crystallization peak obtained at a heating rate of φ and R is the gas constant. The values of E obtained for glass A were 325 and 365 (± 10) kJ/mol for the first and second crystallization peaks, respectively. These values of E are comparable

with those for common silicate glasses such as $Li_2O.2SiO_2$ (E = 300 kJ/mol) or $Na_2O.2CaO.3SiO_2$ (E = 370 kJ/mol). This similarity in E suggests that this particular iron phosphate glass (glass A) has a resistance to crystallization comparable to that of the common silicate glasses. Similar measurements are continuing for other iron phosphate glasses to determine E as a function of composition (iron content) as well as the Fe(II) content in the glass.

3.5.2. Iron Phosphate Glasses Containing Na_2O, Cs_2O, Bi_2O_3, or UO_2:

Studies on glass formation and crystallization of iron phosphate glasses containing Na_2O, Cs_2O, Bi_2O_3, or UO_2 have also been undertaken since these oxides are commonly found in most radioactive wastes. The DTA measurements at a heating rate of 10° C/mm in nitrogen have been completed for the following glasses.

1. $(100-x)(31Fe_3O_4\text{-}69P_2O_5)\text{-}x(Na_2O)$, x = 5.2, 10.2, and 14.9, mol%
2. $(100-x)(40Fe_2O_3\text{-}60P_2O_5)\text{-}x(Cs_2O)$, x = 9.6, 11.7, 13.7, 15.6, 17.4, 24, 27, and 29.7 mol%
3. $(100-x)(40Fe_2O_3\text{-}60P_2O_5)\text{-}x(Bi_2O_3)$, x = 1, 3, 7, and 10, mol%
4. $(100-x)(31Fe_3O_4\text{-}69P_2O_5)\text{-}xUO_2$, x = 5.2, 9.9, and 15, mol%.

The DTA results are now being analyzed and the phases crystallizing from these glasses are being identified by XRD. Preliminary results suggest that the glass formation tendency of glass B (Table II) increases slightly when doped with up to 5 mol% Na_2O (series 1). Further increases in Na_2O causes the DTA crystallization peak to become larger and sharper, and shifts it to lower temperature, indicating an overall increase in the tendency for crystallization. Adding Cs_2O to glass A (series 2) increases its glass forming tendency up to 11.7 mol% Cs_2O, but further increases in Cs_2O lower the glass formation tendency. A similar effect was also observed when glass A was doped with Bi_2O_3 (series 3). The DTA results show an improvement in glass formation when just 1 mol% Bi_2O_3 is added to glass A, but further additions of Bi_2O_3 decrease the glass forming tendency or increases the crystallization tendency of this glass.

For any of the UO_2 containing glasses (series 4), no sharp DTA crystallization peak was observed when heated at 10° C per minute. Only a slow change in slope of the DTA thermogram, which is presumed due to crystallization, appears at-about 670" C which is much higher than the crystallization temperature, about 580" C, of the undoped glass B. These results indicate that the

crystallization tendency is much less (or glass formation tendency is high) when UO_2 is present in this glass. Along with the detailed analyses of the DTA results, work is continuing to investigate the structural role of these oxides in the iron phosphate glasses using XRD, Mossbauer, XPS, XANES, and EXAFS.

3.6. Corrosion of Refractory Materials in Iron Phosphate Melts.

To identify a suitable refractory material for large scale and continuous melting of iron phosphate glasses, studies on the corrosion resistance of different refractories to these melts have been undertaken. Approximately 200g of the melt was placed in a platinum crucible at a desired temperature. The refractory test specimen, in the form of a cylindrical rod (about 0.5" in diameter and 4" long) was immersed about half way in the melt through a hole in the top of the furnace. The test rod was attached to a variable speed motor and rotated at a speed of about 10 rpm for about 24 h. At the end of the experiment, the refractory rod was removed from the melt, held above the melt inside the furnace for about 10 min to allow the melt adhering to the surface of the rod to drip into the melt and then quickly transferred to an annealing furnace to avoid breakage due to thermal shock.

The diameter of the rod at the melt line and at a distance half way down from the melt line was measured and compared with the initial, uncorroded diameter. The corrosion rate was determined from $(d_f - d_i)/2$ per day (24 h), where d_f and d_i are the final (corroded) and initial (uncorroded) diameter of the rod, respectively. The values of d were determined from the average of four different measurements at a particular position of the rod.

The corrosion rate of five different refractories (Coors AD998 alumina, Corhart-ZS-1300, Emhart-333, Z-Aac, and Fusilac-C) in the melt of composition A (melting temperature about 1000" C) at 1270" C is shown as bar graphs in Fig. 12. The results show that these refractories generally have low corrosion rates in melt A, especially Z-Alac and Corhart-ZS-1300. These results are encouraging. As expected, the corrosion rate for all the specimens was always higher at the melt line compared to that at a level half way down from the melt line. With the exception of Fusilac-C, all the other refractories investigated are considered suitable for use as a crucible for melting this iron phosphate glass.

Similar corrosion measurements were also conducted at 1270° C for the Z-Alac, Corhart-ZS-

1300, and Coors AD998 alumina refractories in the melt of an iron phosphate wasteform containing 50 wt% of a Hanford C-112 sludge which contained about 30 wt% of UO_2. The actual melt composition, wt%, was $54.5P_2O_5$, $10.0Fe_2O_3$, $2.0Al_2O_3$, 8.0CaO, $4.5Na_2O$, 4.8NiO, $1.2SiO_2$, $15UO_2$. The melt line corrosion rates of these refractories are shown and compared with those in the melt of composition A in Fig. 13. The C-112 wasteform melt is obviously more corrosive toward these refractories than melt A. Like that in the melt A, the Corhart-ZS-1300 refractory shows a small corrosion rate (about 0.3 mm/day) in the C-112 wasteform melt.

The investigation of the corrosiveness of different iron phosphate melts toward various refractories will continue. Contact has been made with Corhart Refractories who have agreed to supply at no cost different type of refractory materials that are used for constructing glass melting furnaces. In addition to measuring the corrosion rate, attempts will be made to investigate the reaction occuring at the melt-refractory interface by cutting the corroded rods into half-cylinders and examining the interface by SEM and EDAX.

IV. SECOND YEAR WORK PLAN

During the second year of this project, we will focus mainly on iron phosphate glasses containing simulated HLW components. Also, we will complete the analysis of Mössbauer, neutron diffraction, XAS and XPS data we have already collected on binary iron phosphate glasses. Our goals for the second year are:

6. Prepare iron phosphate glasses containing varying concentrations of one or more waste components such as HfO_2 (surrogate for Pu), UO_2, SrO_2, Na_2O, Bi_2O_3, and Cs_2O.
7. Measure critical physical properties such as the chemical durability and glass transition and crystallization temperatures.
3. Develop melting processes which will optimize the critical properties of iron phosphate glasses containing waste components.
4. Investgate corrosiveness of iron phosphate melts containing different waste components toward various refractories. Study the corrosion reactions at the melt-refractory interface for various melt refractory combinations.
5. Use Mössbauer spectroscopy to study the redox equilibria attained during melting and to

investigate how the structural role of iron ions are influenced by the addition of waste components.

6. Probe the near neighbor environment of oxygen ions using x-ray photoelectron spectroscopy.
7. Continue collaborating with *Lawrence Berkeley National Laboratory* and *Stanford Synchrotron Radiation Laboratory* to use x-ray absorption spectroscopy (EXAFS and XANES) to study the local environment around iron ions and various waste ions.
8. Work with scientists from *Argonne National Laboratory* to probe the intermediate and long range order in iron phosphate waste glasses using neutron diffraction and differential anomalous scattering and also to conduct Raman studies.
9. Investigate the effects of radiation on iron phosphate waste glasses in collaboration with scientists from *Pacific Northwest National Laboratory* and *Naval Research Laboratory.*

V. REFERENCES

1. D. G. Rancourt and J. Y. Ping, Nucl. Instr. and Meth. B58 (1991) 85.
2. D. S. Goldman and D. W. Brite, J. Am. Cer. Soc., **69,** 411 (1986).
3. S. I. Zabinsky, A. Ankudinov, J. J. Rehr and R. C. Albers, Phys. Rev. B, 52 (1995) 2995.
4. J. Wong, F. W. Lytle, R. P. Messmer and D. H. Maylotte, Phys. Rev. B, 30 (1984) 5596.
5. G. K. Marasinghe, M. Karabulut, C. S. Ray, D. E. Day, C. H. Booth, P. G. Allen, and D. K. Shuh, Accepted for publication in the J. Amer. Cer. Soc.
6. G. K. Marasinghe, M. Karabulut, C. S. Ray, D. E. Day, W. B. Yelon, C. H. Booth, P. G. Allen, and D. K. Shuh, Accepted for publication in J. Non-Cryst. Solids.

VI. PROJECT PARTICIPANTS

6.1 University of Missouri-Rolla

Dr. Delbert E. Day, Curator's Professor (Project Director)

Dr. Chandra S. Ray, Research Professor

Dr. Kanishka Marasinghe, Research Assistant Professor

Mr. Mevlut Karabulut, Graduate Student (Doctoral Candidate)

Mr. Xiangyu Fang, Visiting Scholar

Mr. Fuyi Chen, Visiting Scholar

6.2 Collaborators

1. Drs. David K. Shuh and P. G. Allen, Actinide Chemistry Division, *Lawrence Berkeley National Laboratory,* CA.

   EXAFS and XANES studies at the *Stanford Synchrotron Radiation Laboratory.*

2. Drs. Marie-Louise Saboungi and David Price, Materials Science Division, *Argonne National Laboratory,* IL.

   Neutron Diffraction Studies and Differential Anomalous Neutron Scattering studies at the Intense Pulsed Neutron Source.

8. Dr. Marcos Grimsditch, Materials Science Division, *Argonne National Laboratory,* IL.

   Raman/NMR studies.

9. Dr. William Weber, *Pacific Northwest National Laboratories,* Richland, WA.

   Radiation damage in iron phosphate glasses.

10. Dr. Dave Griscom, *Naval Research Laboratory,* Washington DC.

    ESR studies of iron phosphate glasses.

VII. PUBLICATIONS AND PRESENTATIONS

7.1. Publications

1. "Redox Characteristics and Structural Properties of Iron Phosphate Glasses:A Potential Host Matrix for Vitrifying High Level Nuclear Waste," G. K. Marasinghe, M. Karabulut, C. S. Ray, D. E. Day, C. H. Booth, P. G. Allen, and D. K. Shuh, In Press, J. Amer. Cer. Soc.
2. "Structural Features of Iron-Phosphate glasses," G. K. Marasinghe, M. Karabulut, C. S. Ray, D. E. Day, W. B. Yelon, C. H. Booth, P. G. Allen, and D. K. Shuh, In Press, J. Non-Cryst. Solids.
3. "On- the Structure and Radiation Chemistry of Iron Phosphate Glasses: New Insights from Electron Spin Resonance and Evolved Gas Mass Spectroscopy," D. I. Giscom, C. I. Merzbacher, N. E. Bibler, H. Imagawa, M. Mesko, and G. K. Marasignhe, Submitted for publication in the proceedings of the 1997 Radiation Effects on Insulators Conference.

7.2 Presentations

1. "Structural Properties of Iron-Phosphate glasses, " March Meeting of the American Physical Society, Kansas City, MO, March 1997.
2. "Redox Characteristics and Structural Properties in Iron Phosphate Glasses: A Potential Host Matrix for Vitrifying of High Level Nuclear Waste," Symposium on Waste Management Technologies and the Ceramic and Nuclear Industries, Annual Meeting of the American Ceramic Society, Cincinnati, Ohio, May 1997.
3. "Structural Features of Iron Phosphate Glasses," 14^{th} University Conference on Glass Science, Bethlehem, PA, June 1997.
4. "On the Structure and Radiation Chemistry of Iron Phosphate Glasses: New Insights from Electron Spin Resonance and Evelved Gas Mass Spectroscopy," D. I. Giscom, C. I. Merzbacher, N. E. Bibler, H. Imagawa, M. Mesko, and G. K. Marasignhe, Radiation Effects on Insulators Conference, Knoxville, TN, September, 1997.

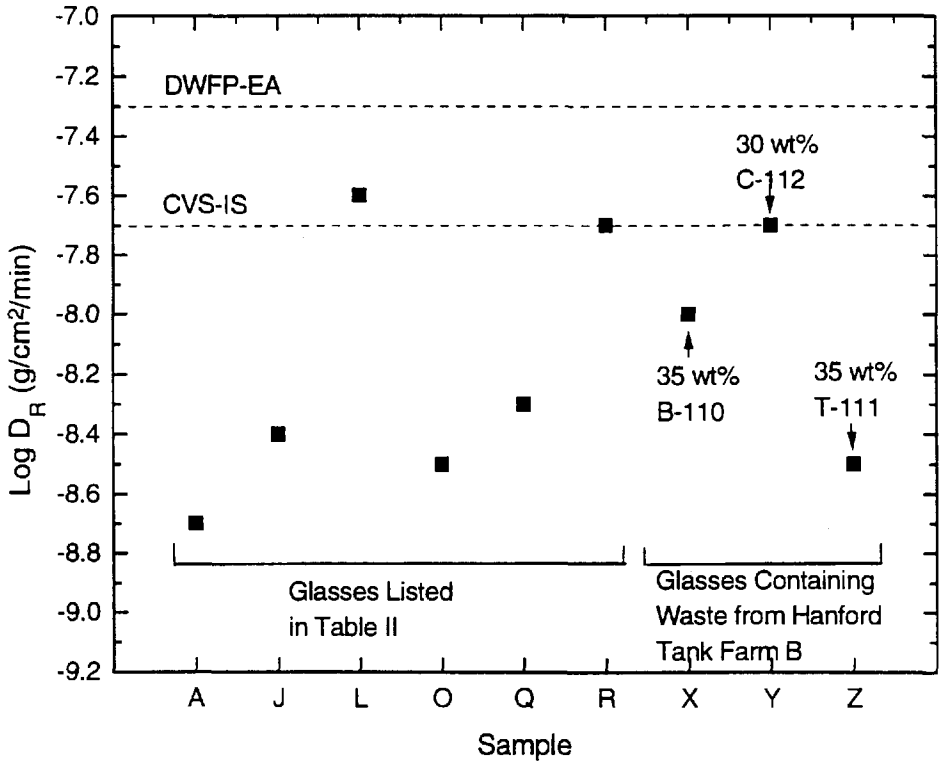

Figure 1. Dissolution rate of several iron phosphate glasses calculated from the weight loss of 1x1x1 cm samples immersed in distilled water @ 90°C for 16 days. Glasses A, J, L, O, Q, and R are described in Table II. Glasses X, Y, and Z contain sludge from three waste tanks designated as B-110, C-112, and T-111, at Hanford, WA. The sludge content in each glass is show in the figure. Dashed lines show the dissolution rate for DWFP-EA and CVS-IS borosilicate silicate standards used at Savannah River, NC and Hanford, WA, respectively.

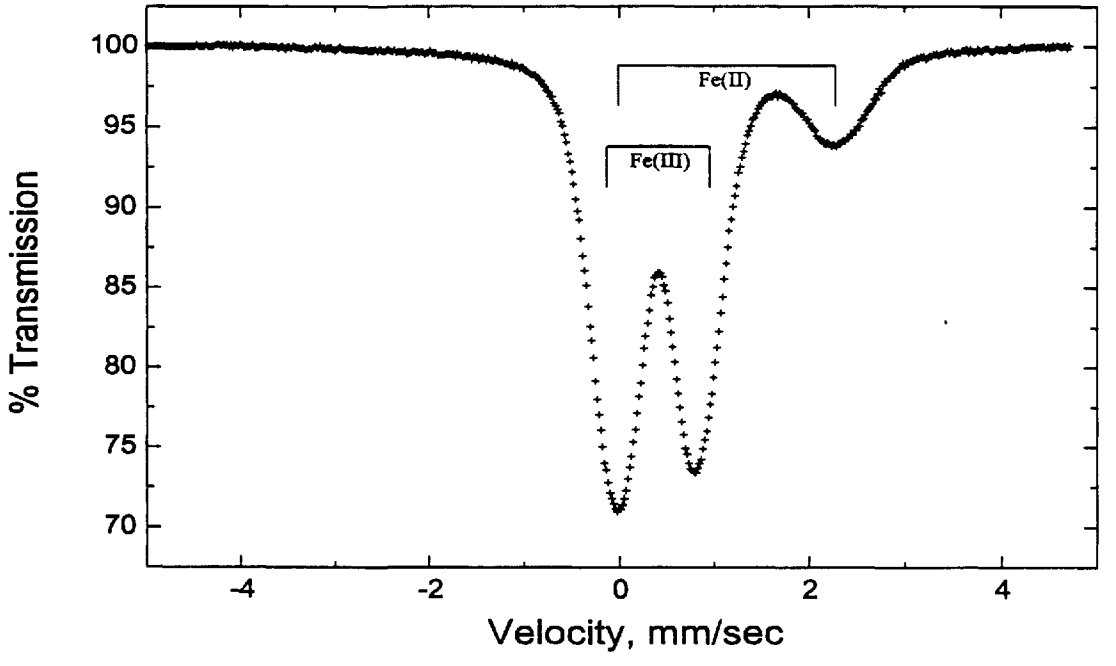

Figure 2. Mössbauer spectrum measured at 295 K of an iron phosphate glass of batch composition $40Fe_2O_3$-$60P_2O_5$(mol%).

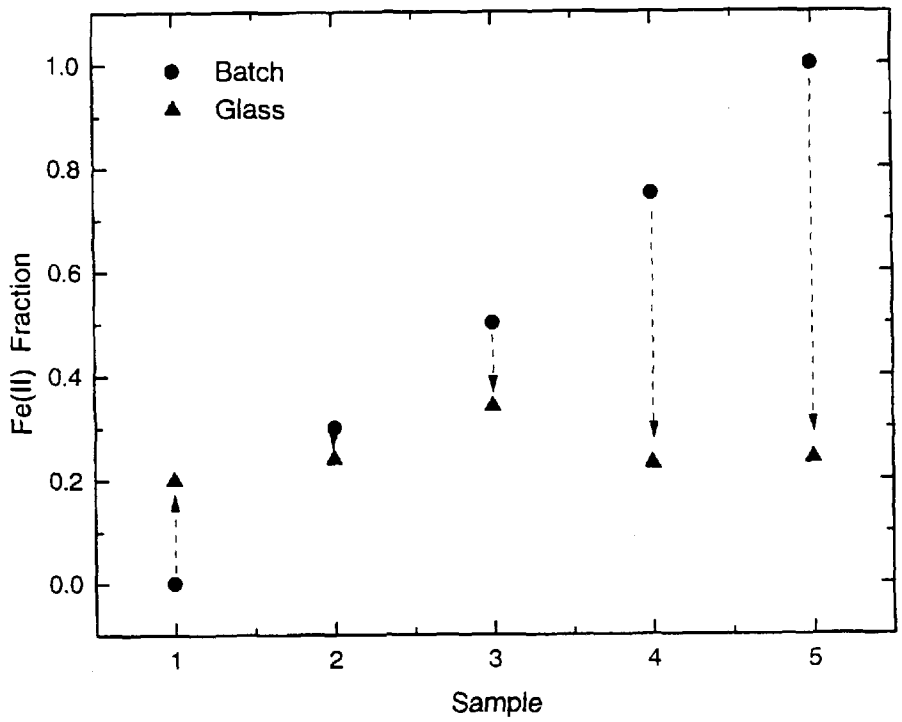

Figure 3. Fraction of Fe(II) in air melted glasses(A) and their batches(O). Fe/P ratio is 0.67 for ail glasses shown above. FeO, Fe_2O_3, Fe_3O_4, or $Fe_2C_2O_4.2H_2O$ or a combination of these iron oxides were used in the batch.

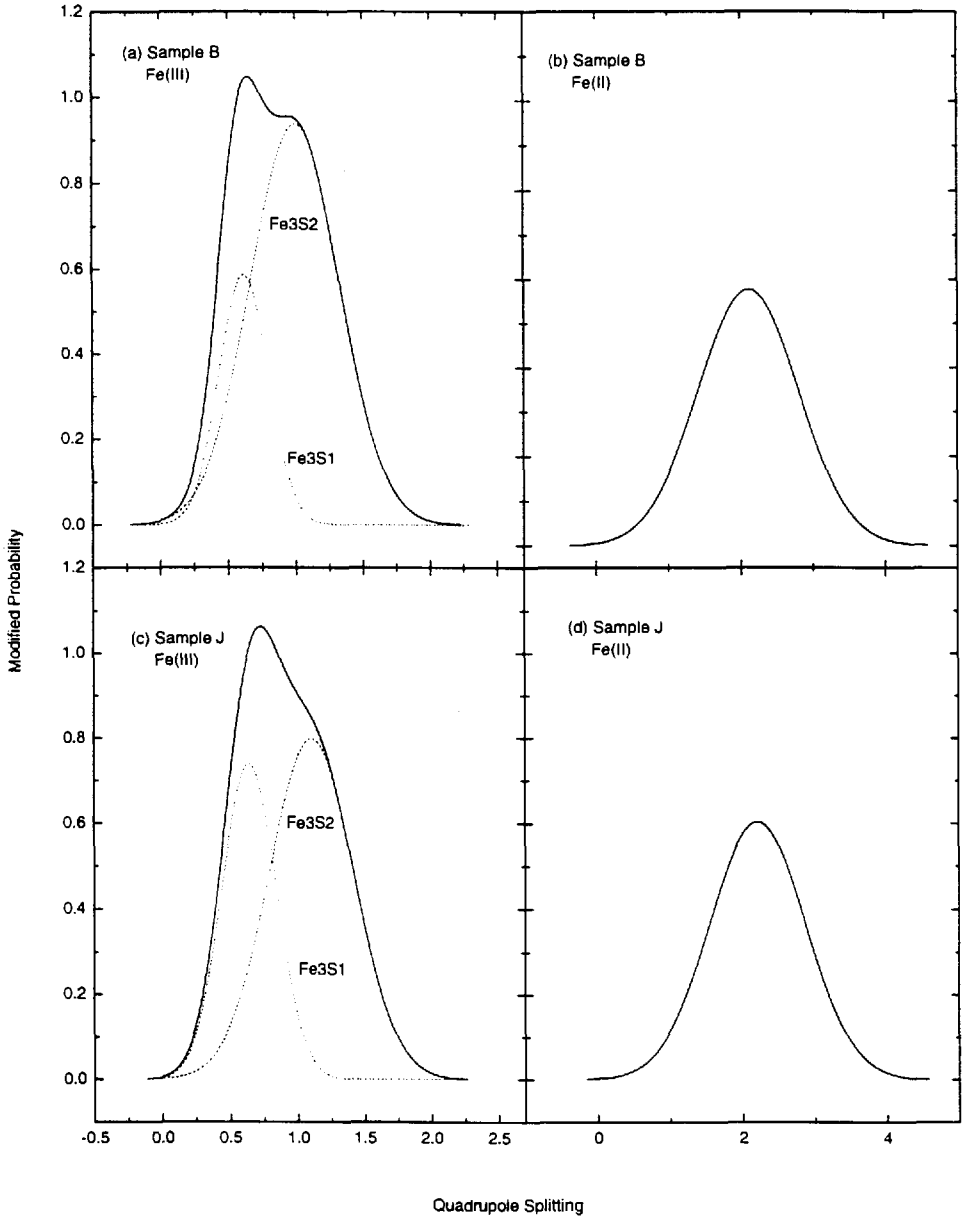

Figure 4. Quadrupole Splitting distributions at iron sites for two iron phosphate glasses containing 23% Fe(II) (a & b) and 40% Fe(II) (c & d).

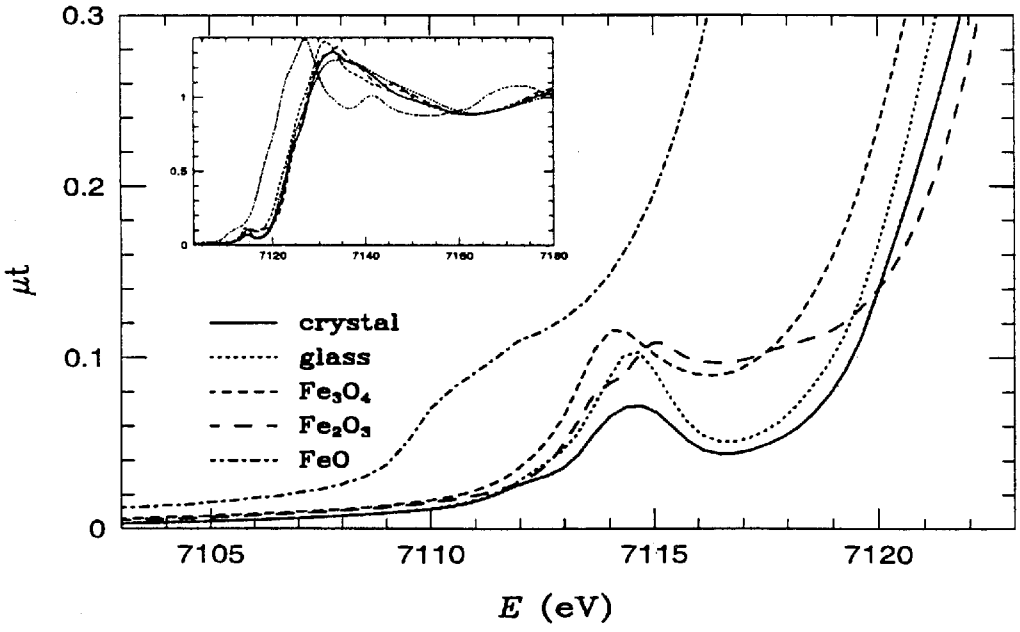

Figure 5. 1s-3d feature in XANES data for a glass with batch composition 31 Fe_3O_4-$69P_2O_5$ (mol%), its crystalline counterpart and several iron oxides.

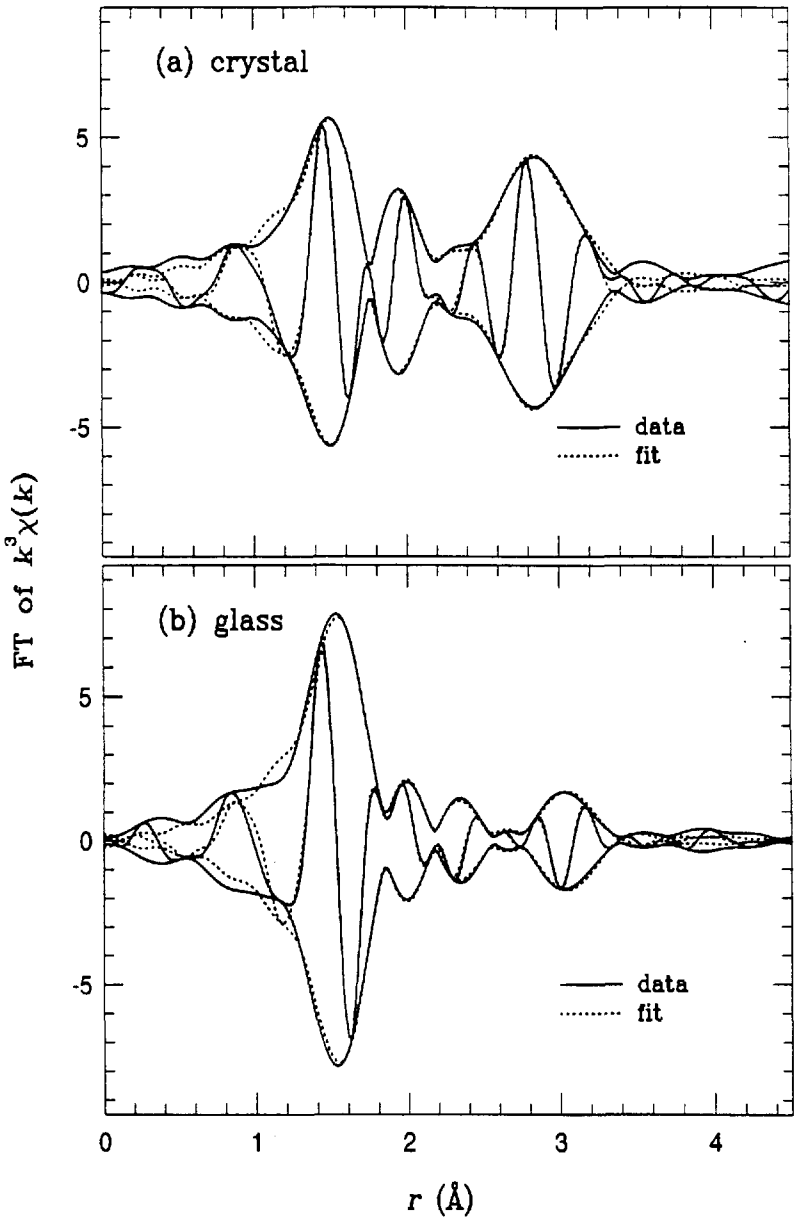

Figure 6. Fourier transform (FT) of $k^3\chi(k)$ for the glass sample B. $31Fe_3O_4$-$69P_2O_5$ (mol%), (bottom) and its crystallized counter part (top). The outer envelope is the amplitude of the transform, and the oscillatory part is the real part of the transform. Peaks correspond to Fe near-neighbors up to a phase shift. For instance, the first peak at 1.5 Å corresponds to oxygen neighbors at ~1.9 Å from the absorbing iron. Transforms are from 4.5-15 $Å^{-1}$ (Gaussian broadened by 0.3 $Å^{-1}$).

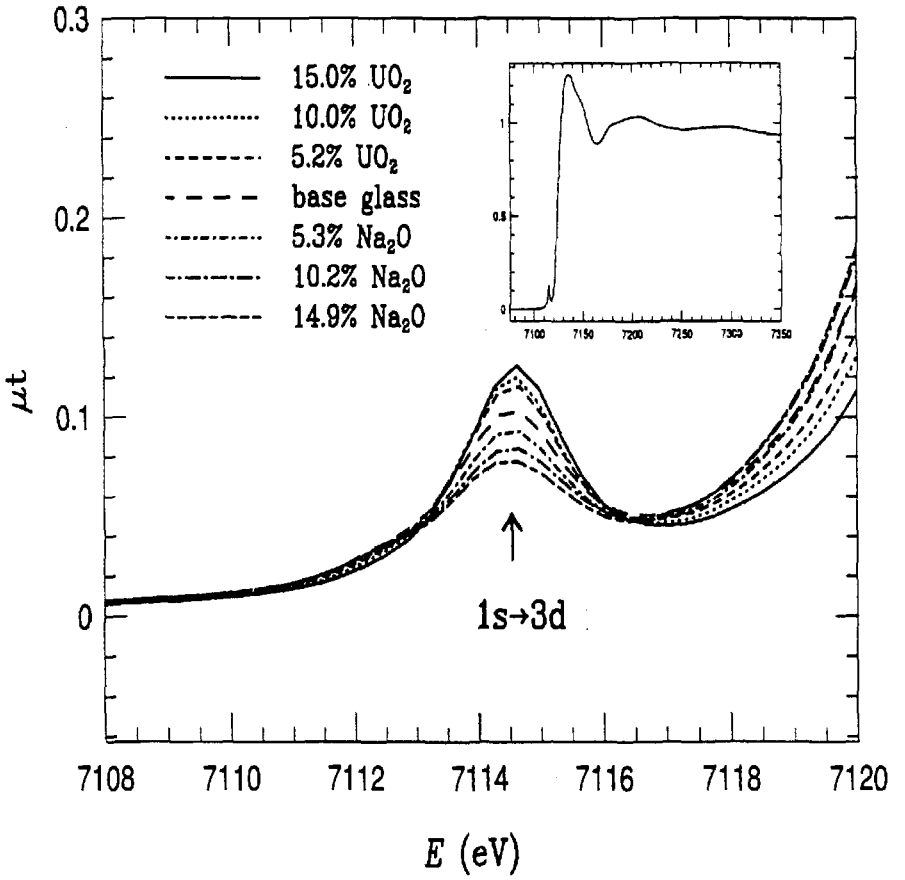

Figure 7. μt (absorption times sample thickness) vs. incident photon energy for iron-phosphate glasses. μt for each spectra is normalized to unity at the edge step for comparison, and energy is defined such that the first inflection point of an Fe foil is at 7112 eV. The main plot is focused on the pre-edge region, where the bump at ~7114.5 eV is due to a 1s→3d transition. Inset shows full edge step for the glass with 15mol% UO_2. Composition of base glass is $31Fe_3O_4$-$69P_2O_5$(mol%).

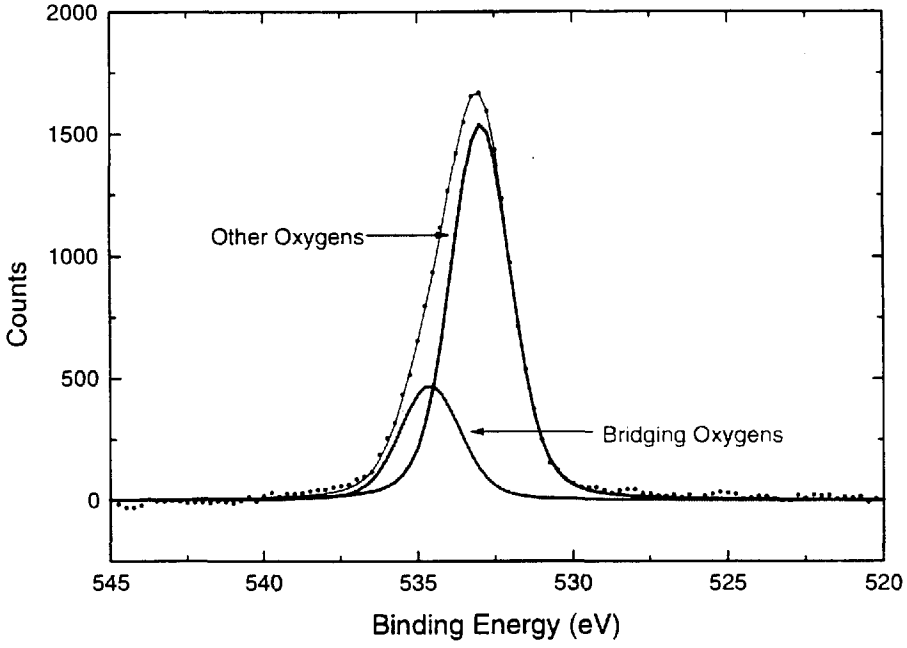

Figure 8. O1s XPS spectrum for an iron phosphate glass whose batch composition was 31Fe_3O_4-69P_2O_5 (mol%).

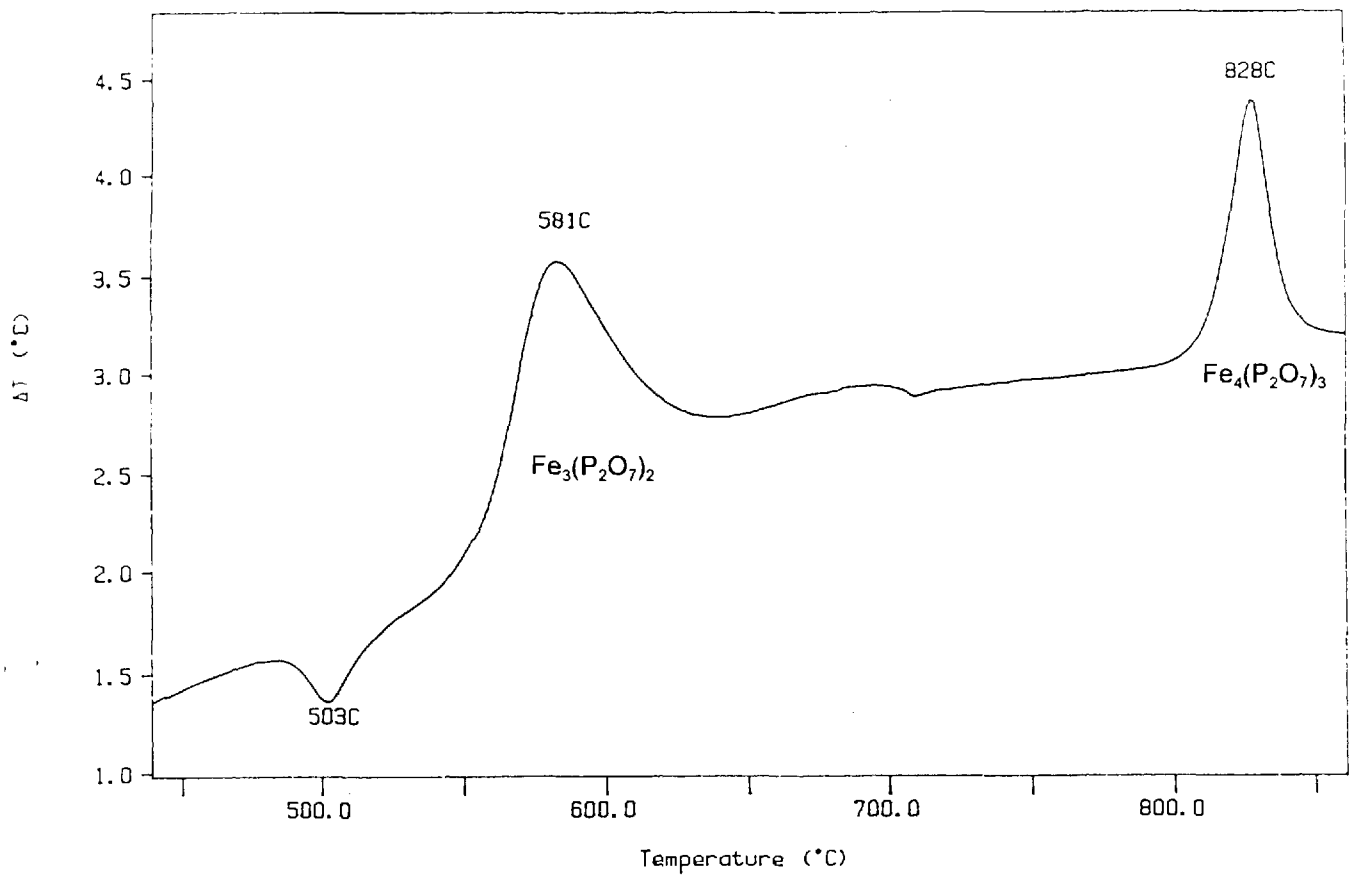

Fig. 9. Differential thermal analysis (DTA) for a $40Fe_2O_3$-$60P_2O_5$, mol%, glass (glass A, Table II) at a heating rate of 10" C/min. Weight of the sample: ~40 mg; Particle size: 25-45 μm; Atmosphere: Flowing (30 cm^3/min) nitrogen gas. Exothermic peaks at 581" C and 828" C correspond to the crystallization of $Fe_3(P_2O_7)_2$ and $Fe_4(P_2O_7)_3$, respectively.

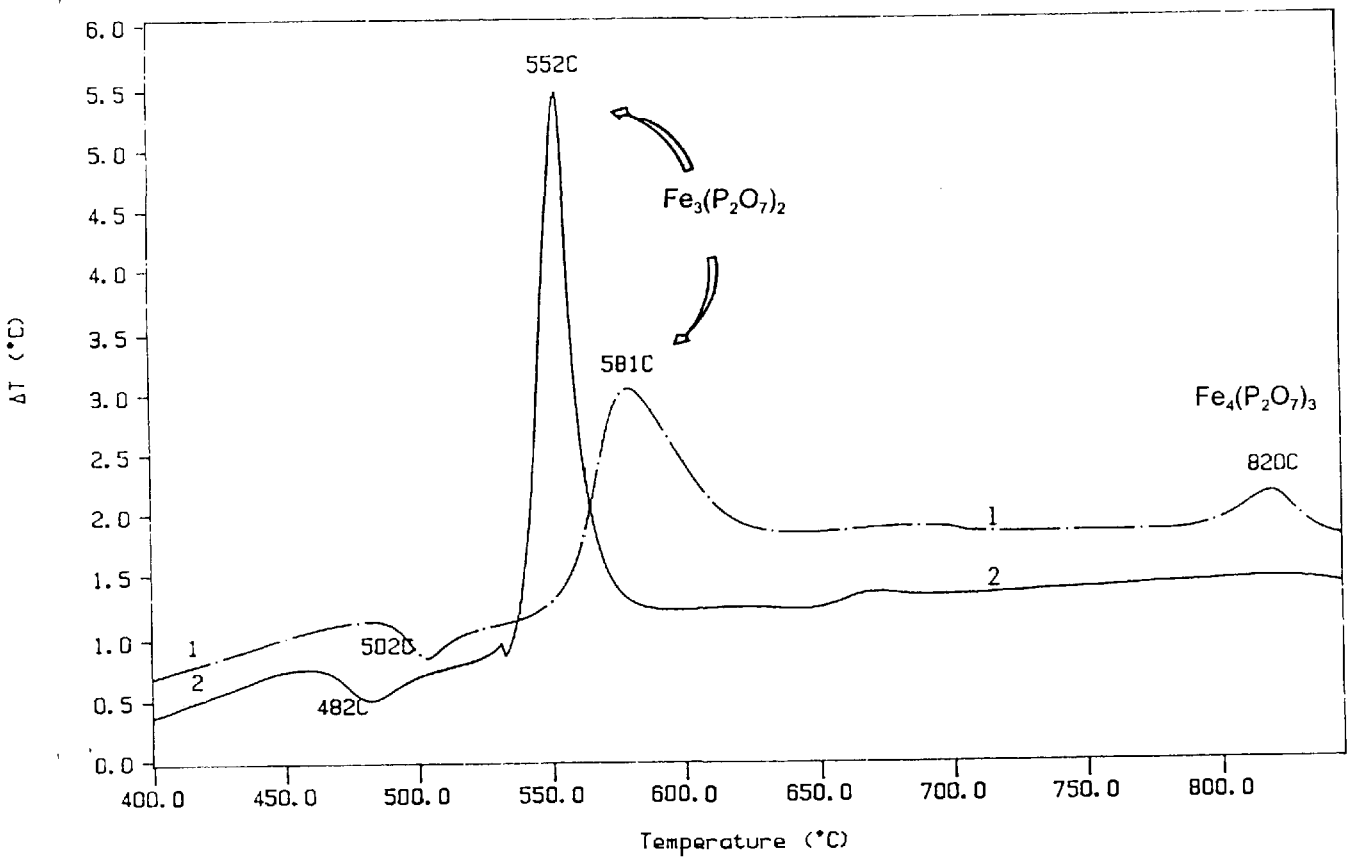

Fig. 10. Differential thermal analysis (DTA) for a (1) $31Fe_3O_4$-$69P_2O_5$, mol% glass (glass B, Table II) (2) glass B preheated at 400" C for 24 h in forming gas, whose Fe^{2+} contents, as measured by Mossbauer spectroscopy, are 25% and 34%, respectively. Weight of the samples: ~40 mg; Particle size: 25-45 pm; DTA heating rate: 10" C/min; Atmosphere: Flowing (30 cm^3/min) nitrogen gas. The first exothermic peak, due to the crystallization of $Fe_3(P_2O_7)_2$, appears at a lower temperature and becomes larger and sharper with increasing Fe^{2+} content in the glass. The exothermic peak at 820" C in (1), which is due to the crystallization of $Fe_4(P_2O_7)_3$, decreases in size with increasing Fe^{2+} and disappears when Fe^{2+} content exceeds 33.3%. Also, compare the DTA thermogram in (1) with that shown in Fig. 9 for glass A whose Fe^{2+} content is about 19%.

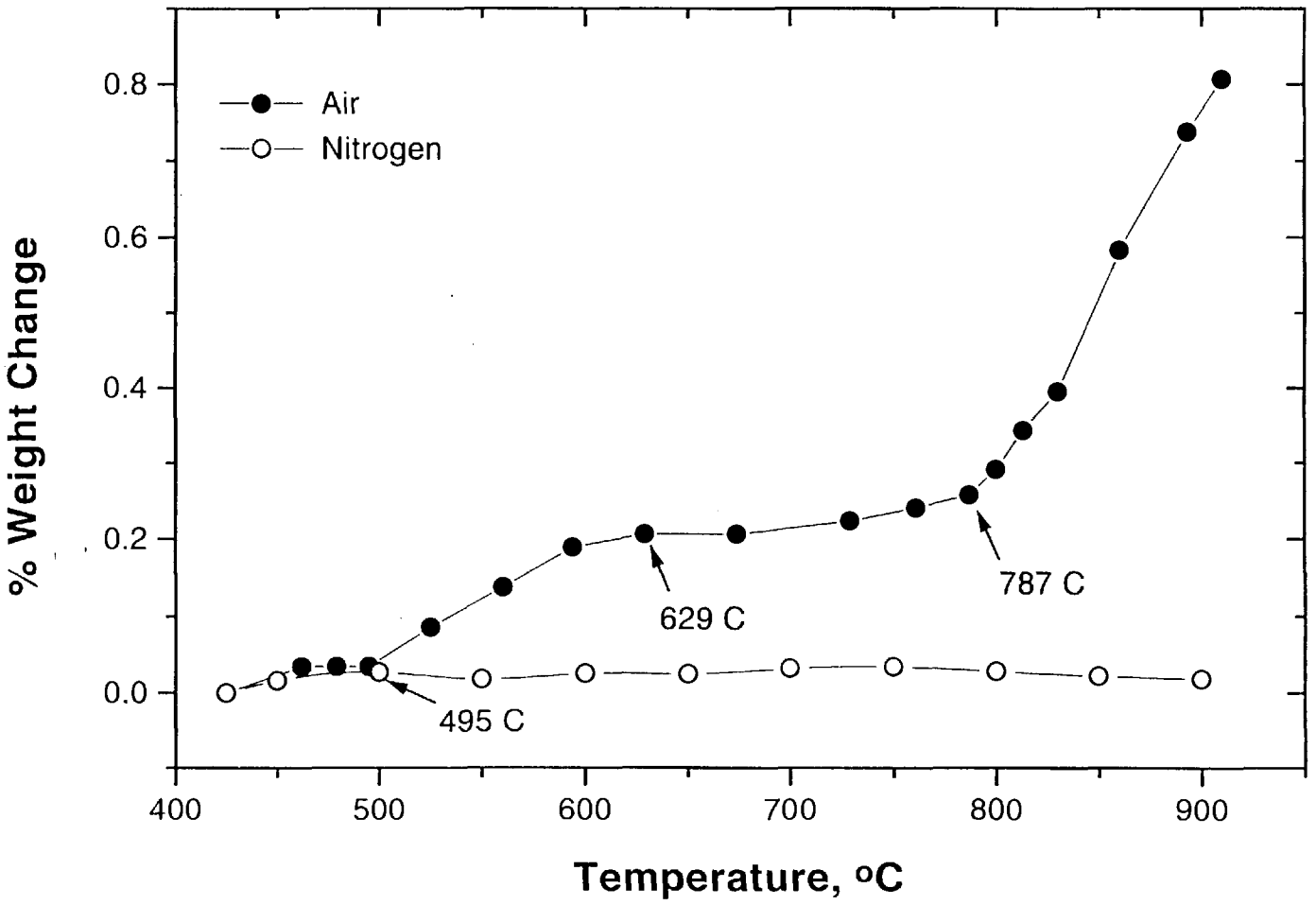

Fig. 11. Thermogravimetric analysis (TGA) for a 3 1Fe_3O_4-69P_2O_5, mol% glass (glass B, Table II) in air and nitrogen at a heating rate of 10" C/min. Weight of the sample: 291 mg; Particle size: 25-45 pm. TGA for this glass conducted in air shows a weight gain (solid circles) which is believed to be by the reaction of the glass with oxygen as Fe^{2+} is oxidized to Fe^{3+}. No such weight gain is observed in the TGA conducted in nitrogen (open circles).

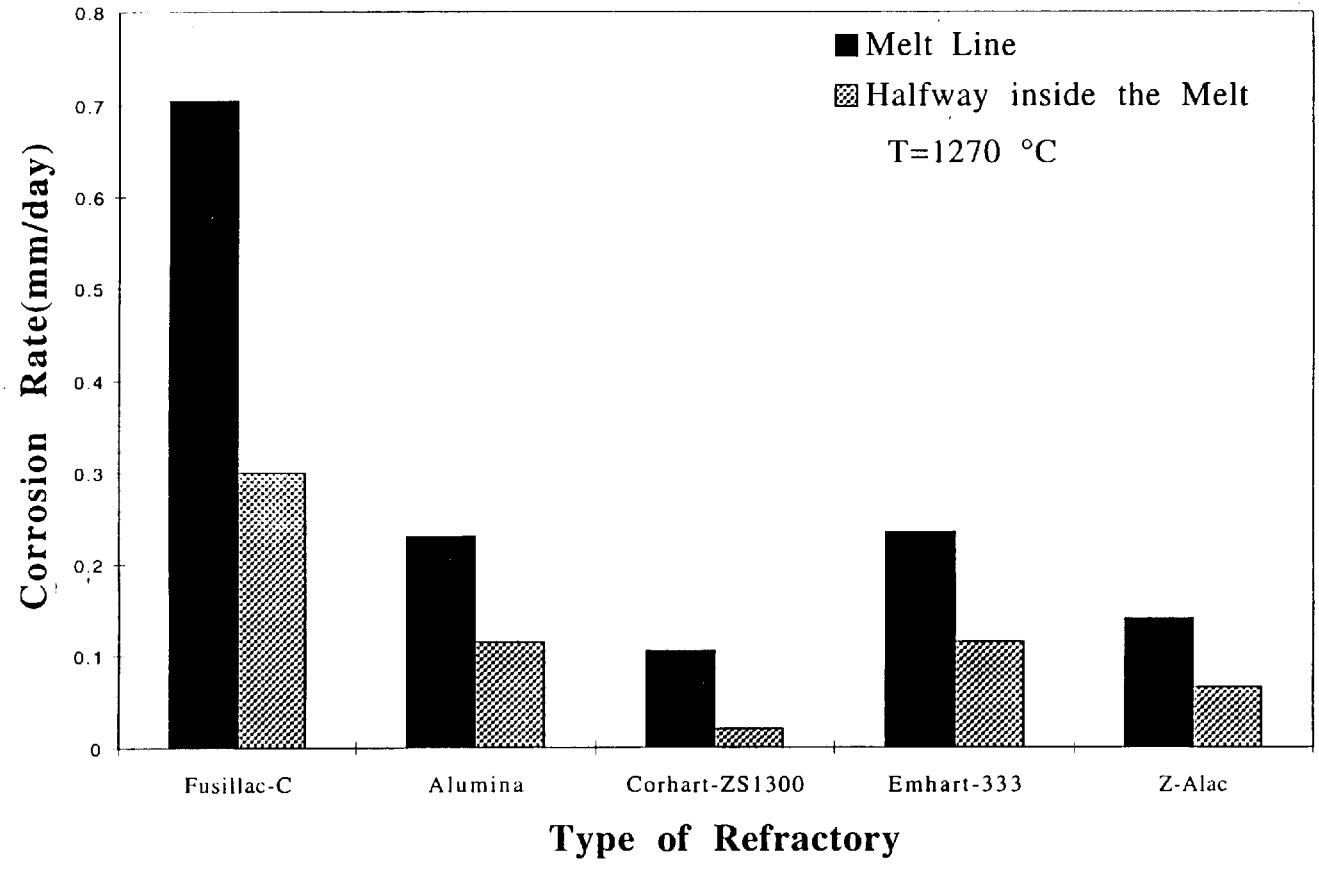

Fig. 12. Corrosion rate for different refractories rotated in molten $40Fe_2O_3$-$60P_2O_5$, mol%, Table II, at 1270° C. While the corrosion rate of Corhart-ZS 1300 in this melt is the lowest and that of Fusillac-C is the highest, the corrosion rates for all these refractories are considered generally low in this melt.

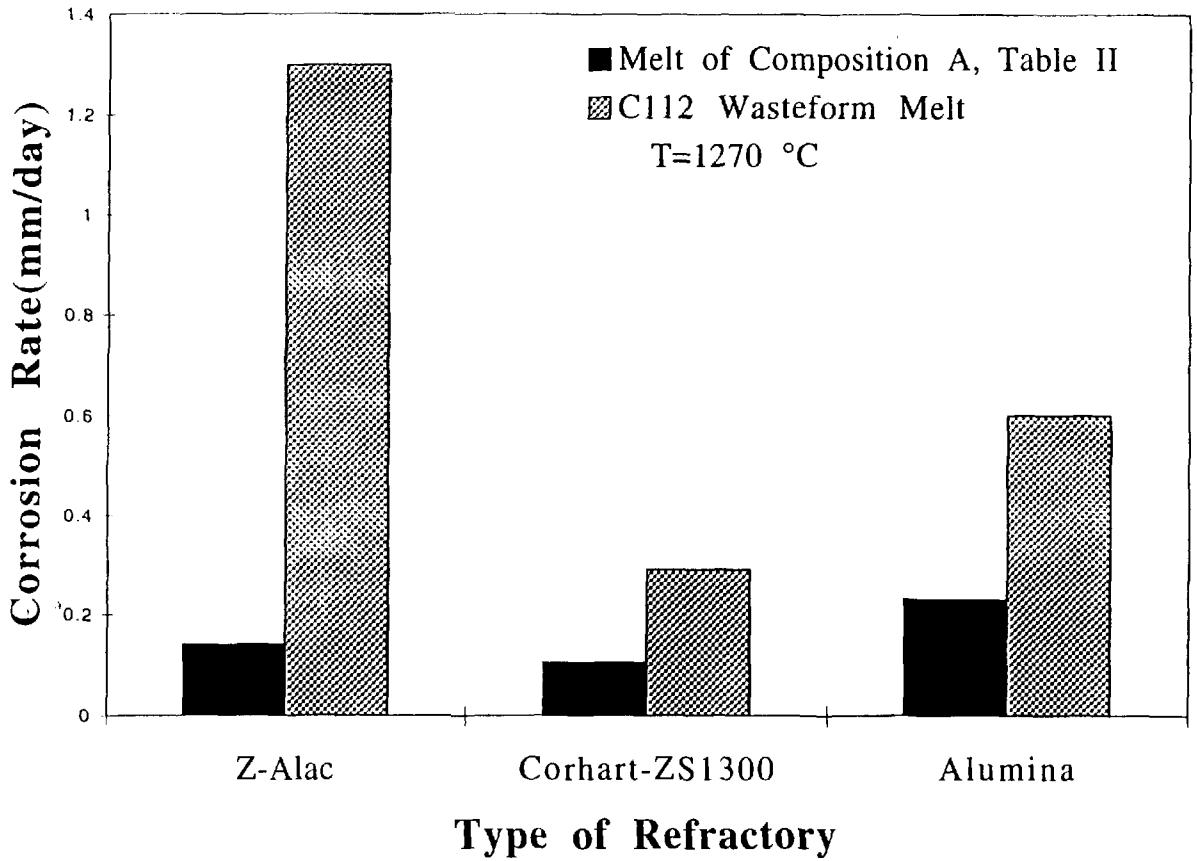

Fig. 13. Comparison of melt-line corrosion rates for different refractories in molten composition A and in an iron phosphate melt that contains 50 wt% of the Hanford C-112 waste. See text for melt compositions. Corrosion was measured at a melt temperature of 1270° C. The corrosion rate in the C-112 wasteform melt is consistently higher than that in melt A for all the refractories.